Cosmic ray angular distribution dynamics during Forbush decrease in 3-4 November 2021

Petr Yu. Gololobov [ID], Vladislav G. Grigoryev [ID], Sardaana K. Gerasimova [ID],
Sergey A. Starodubtsev [ID] , Anton S. Zverev [ID]

Correspondence

Yu. G. Shafer Institute of Cosmophysical Research and Aeronomy, Siberian Branch of the Russian Academy of Science, Russia, gpeter@ikfia.ysn.ru

Abstract

On November 3-4, 2021, there was a coronal ejection of the solar mass into the interplanetary medium. According to direct observations of the interplanetary magnetic field and the solar wind, the ejection was accompanied by a magnetic cloud. During the event, neutron monitors of the NMDB network registered a two-stage Forbush decrease with a total amplitude of up to 15%. A preliminary analysis of the NMDB data shows that the first step was due to the cosmic ray decrease behind the shock wave front, while the second step was due to the cosmic ray anisotropy formed in the magnetic cloud. This work was undertaken to study the dynamics of the angular distribution of cosmic rays in this event. The cosmic ray distribution was determined using the global survey method developed at the ShICRA in the 1960s. The method makes it possible to use the worldwide network of neutron monitors as a single multidirectional instrument and to determine the hourly dynamics of CR distribution. It is shown that unidirectional and bidirectional anisotropies of significant amplitude are observed inside the magnetic cloud. The results obtained are discussed in the framework of modern theories of the formation of magnetic clouds. The temporal dynamics of the spatial-angular distribution of cosmic rays during the Forbush decrease on November 3–4, 2021 was determined. The presence of cosmic ray anisotropy with an amplitude comparable to the magnitude of the density decrease itself was found.

1. Introduction

The flux of galactic cosmic rays (CR) coming from the interstellar medium into the heliosphere fills its entire cavity. The spatial-time distribution of CR at each point of the heliosphere is determined by its properties and structure, which depends on solar activity. Thus, in the interplanetary medium, a special CR angular distribution is formed, which is characterized by both isotropic and anisotropic components. And although the anisotropy is two orders of magnitude lower than the isotropy, it carries a valuable information about the features of GCR modulation by the solar wind.

Of particular interest are sporadic manifestations of solar activity accompanied by a large energy release into the space surrounding the Sun. One of the most striking examples of these processes are coronal mass ejections (CME). As a rule, at the moments of the passage of the Earth's by CME, the so-called Forbush decrease (FD) is observed in the data of ground-based detectors, i.e., sharp decreases in the GCR intensity followed by a gradual recovery. As a rule, on Earth, such an effect is manifested by a single sharp decrease in intensity and its subsequent gradual recovery. However, in some cases, FD can have a multi-stage time profile formed due to the so-called magnetic clouds (MC) propagating in the CME body (Xu et al. 2010). MCs are characterized by a strong regular field, which is capable of shielding GCRs, leading to a decrease in CR intensity and the formation of high-amplitude CR anisotropy (Belov et al. 2015).

2. Forbush decrease during 3-4 November 2021

On November 2, 2021, an M7.1 class solar flare occurred according to the SOHO spacecraft, as a result of which a high-velocity CME ejection was observed from the AR2891 active region (https://cdaw.gsfc.nasa. gov/CME_list/UNIVERSAL/2021_11/univ2021_11.html, last accessed June 27, 2023), which later overtook the CMEs that occurred on November 1-2 with slow velocities. As a result, according to the data of direct measurements of spacecraft (Figure 1), an interplanetary CME was observed on November 3-4. The arrival of the CME shock wave front to the observation point, which is located in close proximity to the Earth at the libration point L1, at 2021-11-03 20:00 was accompanied by a sharp jump in pressure and velocity of the solar wind, as well as an increase in the interplanetary magnetic field (IMF) module, followed by an increase in the IMF turbulence level. In the period from 2021-11-04 12:00 to 2021-11-05 04:00 , a decrease in the field turbulence level and a gradual decrease in the solar wind velocity were observed, accompanied by a gradual change in the direction of the field vector. The behavior of the IMF and solar wind parameters allows us to conclude that the passage of MC was observed during the above period (Burlaga et al., 1981).

The measurement data of CR from the network of neutron monitors for November 3-6, 2021 is shown in Figure 2. As can be seen, the arrival of the ICME was accompanied by a FD, which had a two-stage character. The first stage corresponds to the moment of arrival of the shock wave to the Earth, and its depth depends inversely on vertical geomagnetic cutoff rigidities of the stations R_c . The second stage of the FD arose at the time of the passage of the MC and has an ambiguous behavior, characterized by a shift in the maximum depth, which, at the same time, does not depend on R_c. This allows us to conclude that a large CR anisotropy was observed inside the MC in this event.

3. Global survey method

To study the dynamics of the spatial-angular distribution of CRs, this work uses the global survey method (GSM) (Altukhov et al. 1970). GSM is the first method for studying the short-term dynamics of the CR angular distribution. Somewhat later, similar methods were developed by various researchers (Belov et al. 2018; Dvornikov & Sdobnov 1998; Bieber & Evenson 1989). GSM is a variant of spherical analysis of CR registration data of the world network of neutron monitors. It allows you to consider the entire global network of CR detectors as one multidirectional detector and instantly determine the CR distribution.
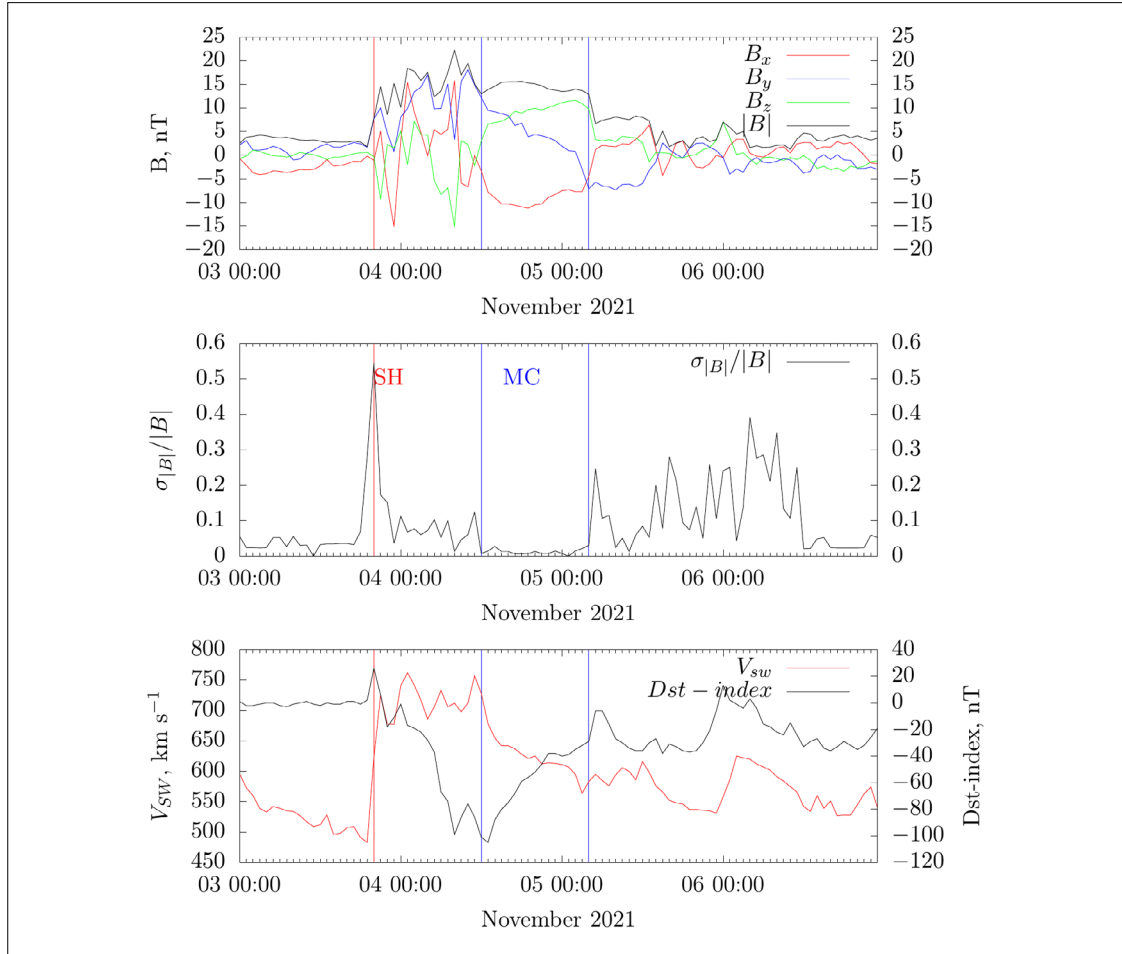
Fig. 1: The values of the components and modulus of the IMF intensity vector B, the field regularity level ($\sigma_{|B|} / B$) and the solar wind velocity V_{SW} and the geomagnetic activity Dst index for November 3-6, 2021 according to the OMNI catalog. The vertical red line corresponds to the moment of arrival of the shock wave to the Earth; the blue vertical lines show the MC boundaries.

Thus, the temporal resolution of determining the CR distribution is limited only by the capabilities of the detector network. In this case, 1-hour measurement data from neutron monitors included in the Neutron Monitor DataBase (NMDB) are used.

The method is based on the so-called receiving vectors (Krymsky et al. 1966), which makes it possible to establish a relationship between CR intensity variations in near-Earth outer space and the intensity of CR recorded by ground-based detectors. We will briefly describe the method below.

The CR distribution over the sphere $I(\theta, \varphi)$ when expanded into a series in terms of spherical harmonics will have the form:

$$I(\theta, \varphi) = \sum_{n=0}^{\infty} \sum_{m=0}^{\infty} (a_n^m \cos(m\varphi) + b_n^m \sin(m\varphi)) P_n^m(\sin\theta), \quad (1)$$

where θ and φ are latitude and longitude angles in the corresponding coordinate system, $P_n^m(\sin\theta)$ are associated Legendre polynomials, $0 \le m \le n \le \infty$.
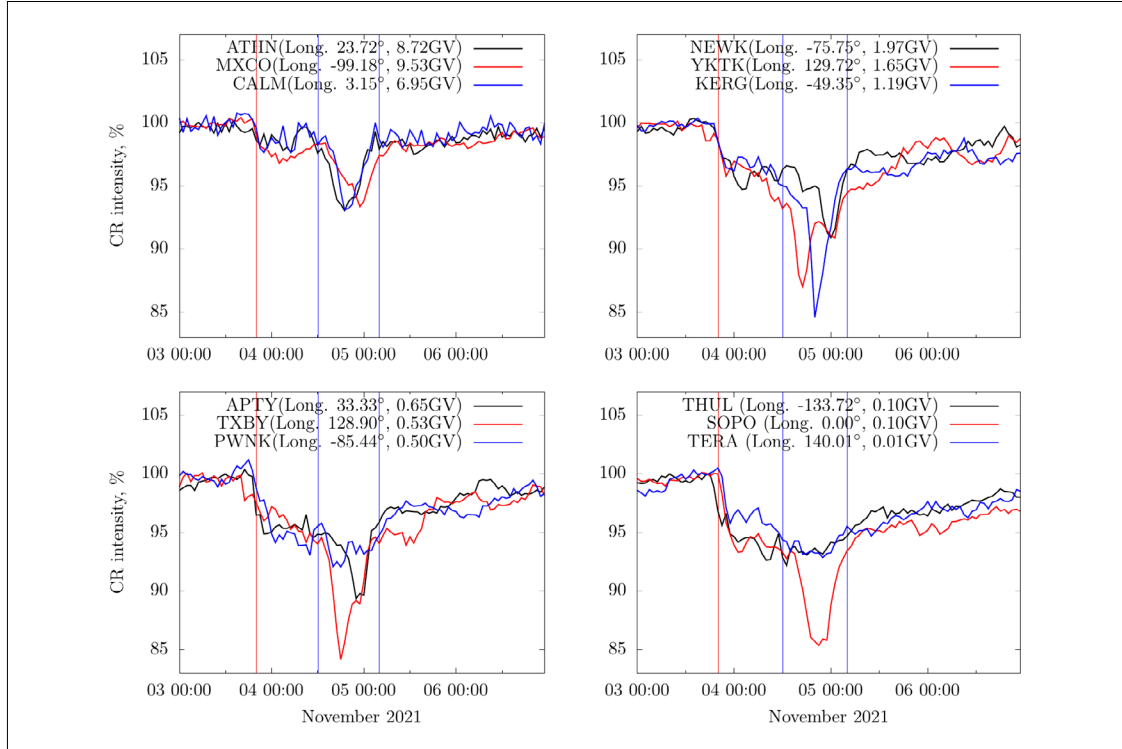
Fig. 2: Relative CR intensity recorded by the global network of neutron monitor stations according to the NMDB database for November 3–6, 2021. The stations are distributed according to the cutoff rigidities R_c. The vertical red line corresponds to the moment of arrival of the shock wave to the Earth, the vertical blue lines show the MC boundaries.

If we represent $I(\theta, \varphi)$ as a multidirectional vector $\overrightarrow{A} = (a_n^m, b_n^m)$ then the CR intensity by an individual ground-based detector will be equal to the product $I = \overrightarrow{A}\overrightarrow{R}$, where $\overrightarrow{R} = (x_n^m, y_n^m)$ is a multidimensional receiving vector.

The receiving vector for a real detector is determined taking into account its directional diagram $N(\theta, \varphi)$, CR trajectories in the geomagnetic field (asymptotic angles of arrival of particles Θ, Φ) and response functions $W(E, \theta)$:

$$
z_n^m = \frac{\int\limits_{R_c}^{\infty}\int_0^{2\pi}\int_0^{\pi/2} W(E,\theta)f_n(E)N(\theta,\varphi)\, e^{im\Psi}P_n^m(\sin\Phi)\sin\theta\, dE\, d\varphi\, d\theta}{\int\limits_{R_c}^{\infty}\int_0^{2\pi}\int_0^{\pi/2} W(E,\theta)f_n(E)N(\theta,\varphi)\sin\theta\, dE\, d\varphi\, d\theta} \, , \tag{2}
$$

where $z_n^m = x_n^m + iy_n^m$, $f_n(E)$ is an energy spectrum of variations of the n-th harmonic.

As can be seen, the receiving vectors strongly depend on the form of the energy spectrum of the variations. In this particular case, it is difficult to determine the dynamics of each $f_n(E)$ during the event we are considering. However, we will rely on previously known studies of energy spectra given in the literature. We present below the spectra we have chosen and the rationale for our choice.

As was shown in (Grigoryev et al. 2014), in the growth phase of solar activity in cycle 24, it was close to a power law with indicators of 1.01±0.07. Also, long-term observations in the work of other authors (Kravtsov & Sdobnov 2013; Alania et al. 2013) show that the power-law form of the spectrum satisfac-

Tab.1: The list of NMDB neutron monitor together with their geographic locations, vertical geomagnetic cutoff rigidities and altitudes.

No.	Neutron monitor station	Latitude, deg.	Longitude, deg.	R_c, GV	Altitude, m a.s.l.
1	ATHN	37.97	23.72	8.72	40
2	MXCO	19.33	-99.18	9.53	2274
3	CALM	40.55	3.15	6.95	708
4	ROME	41.86	12.47	6.32	60
5	AATB	43.14	76.60	6.69	3340
6	BKSN	43.28	42.69	5.60	1700
7	JUNG	46.55	7.98	4.48	3550
8	LMKS	49.20	20.22	4.00	2634
9	IRK3	51.29	100.55	3.66	3000
10	IRKT	52.47	104.03	3.66	433
11	NWRK	39.68	-75.75	1.97	50
12	KIEL2	54.33	10.13	2.29	54
13	YKTK	62.02	129.72	1.65	95
14	KERG	-49.35	70.25	1.19	0
15	OULU	65.02	25.50	0.81	0
16	APTY	67.55	33.33	0.65	177
17	NRLK	69.26	88.05	0.63	0
18	TXBY	71.60	128.90	0.53	0
19	FSMT	60.02	-111.93	0.30	0
20	INVK	68.35	-133.72	0.18	21
21	NAIN	56.55	-61.68	0.40	0
22	PWNK	54.98	-85.44	0.50	0
23	THUL	76.50	-68.70	0.10	260
24	MWSN	-67.60	62.88	0.22	30
25	SOPO	-90.00	0.00	0.10	2820
26	TERA	-66.65	140.01	0.01	45

torily describes the experimental data. Although there are reasons to believe that $f_0(E)$ may have a more complex form (Kravtsova & Sdobnov 2013; Sakakibara et al. 1985), in this paper we will assume that it has a power form with exponent -1.

In a number of works (see e.g. Ahluwalia & Riker 1987; Jacklyn et al. 1970; Pomerantz & Duggal 1971) studies of the energy spectrum $f_1(E)$ have been carried out with the assumption that it has a power-law form $f_1(E) = E^\gamma$. The analysis of long-term experimental measurements of solar-diurnal variations in CR intensity by ground-based detectors, carried out in these works, showed that $f_1(E)$ can be adequately described by a power-law spectrum with an upper cutoff E_u. In this case, the exponent γ turned out to be equal to 0, and E_u, on average for a cycle of solar activity, took values close to 100 GeV. Further, a detailed analysis of $f_1(E)$ showed that the index γ varies in a narrow range from -0.3 to 0.5 (Hall et al.

1997), which also confirmed previous results. This is also confirmed by our latest studies (Gololobov et al. 2021). And although it is very likely that such a flat spectrum with an unexpected cutoff is unnatural, the main thing is that it agrees satisfactorily with experimental data.

Krivoshapkin et al. (1970) assumed that the observed semidiurnal CR variations are due to the screening effect of the regular IMF, which creates an excess of particles from the direction across the field. In this case, the energy spectrum $f_2(E)$ following from this theory has the form E^1 for $E \leq E_O$ and E^{-2} for $E > E_O$, and the characteristic energy was determined by the IMF parameters. An analysis of the experimental data made it possible to estimate at 70 GeV. A similar spectrum and values were also obtained by Zusmanovich and Mirkin (1983). On the other hand, according to the estimates of Ahluwalia and Fikani (1996), the energy spectrum indices were somewhat different values of 0.7±0.3 and −0.4±0.2, and E_O depended on the SA cycle, reaching 50 GeV at the minimum of solar activity and 150 GeV at the maximum. Despite somewhat different estimates of the energy spectrum obtained in the above papers, in general it can be argued that semidiurnal variations in the CR intensity should be observed in the energy region close to 70 GeV.

The first two angular momenta of the CR distribution function are described by 9 components a_0^0, a_1^0, a_1^1, b_1^1, a_2^0, a_2^1, b_2^1, a_2^2, b_2^2 and, respectively, for their determination requires at least 9 equally distributed neutron monitor stations. To implement the GSM for the FD event on November 3–4, 2022, 26 neutron monitor stations were used, providing data at that time to the NMDB. Despite their uneven distribution, the number of stations exceeds the required number by almost 3 times and is sufficient for the implementation of the GSM. The list of stations with their characteristics is presented in Table 1.

4. Results and discussions

The results of the implementation of the GSM are shown in Figure 3. As can be seen, the decrease in the isotropic component of the CR intensity had a two-stage character. The maximum of the first stage of the phase transition practically coincides with the moment of arrival of the shock and is about 5.6%, while the second step of the phase transition has a parabolic time profile and its maximum falls on the center of the MC with an amplitude of 5.3%. Also, inside the MC, there is a sharp increase in the amplitude of both diurnal and semidiurnal CR anisotropy. The maximum modulus of the CR symmetric diurnal anisotropy vector reaches 3.5%, the antisymmetric diurnal one, 5.8%, and the semidiurnal one, 3.4%. Thus, the magnitude of the CR anisotropy in the MC is comparable to the FD itself. This explains the observed fact of inconsistency in the decrease in the NM data, namely, that the second stage of the FD in the data of some neutron monitors was very deep, while in the data of others it was completely absent.

If the spatial direction of vector anisotropy can be described by three components a_1^0, a_1^1 and b_1^1 of the vector in the Cartesian coordinate system, then tensor anisotropy with its 5 components a_2^0, a_2^1, b_2^1, a_2^2 and b_2^2 is hard enough to represent in space. The most obvious visualization of tensor anisotropy is the tensor ellipsoid, also defined by 5 components: three semi-axes and two angles that determine the direction of one of the semi-axes. Representing it in this form, let us consider the temporal dynamics of the direction of the ellipsoid's greatest semi-line and the direction of the IMF during the passage of the CME.

The results obtained are presented in Figure 4. As can be seen, the CR tensor anisotropy amplitude has reached maximum values of the order of ~7% at minimum values of isotropic intensity. This moment of time corresponds to the moment when the Earth passes through the central region of the MC. The time
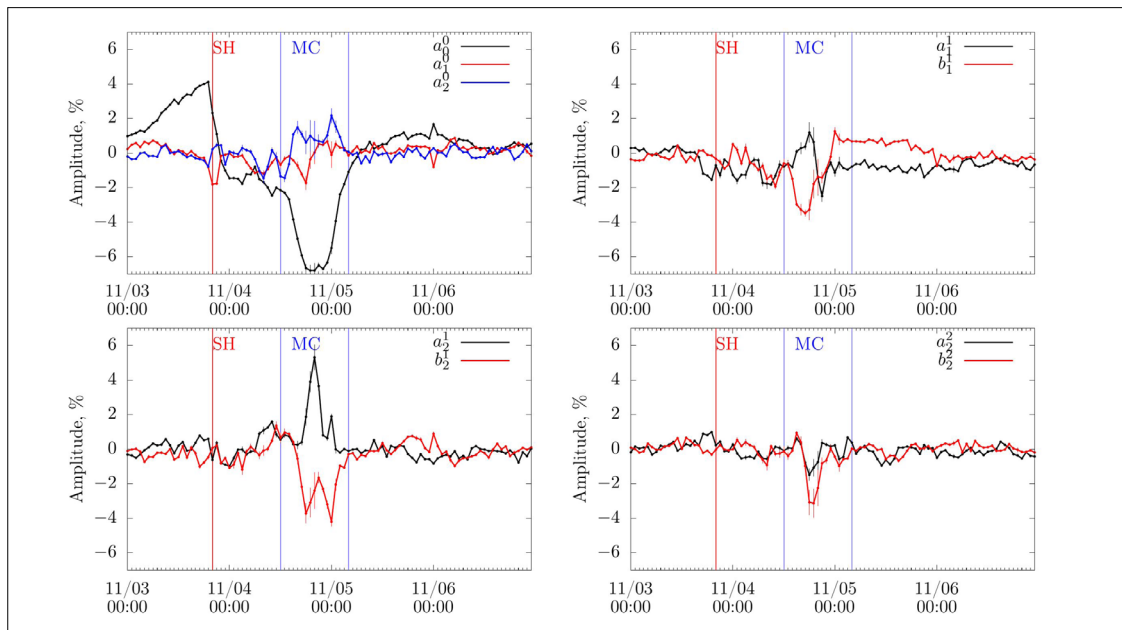
Fig. 3: The parameters of the first two spherical harmonics of the angular distribution of CR obtained using the GSM for November 3–6, 2021. The moments of arrival of the shock wave and the MC boundaries are indicated by red and blue vertical curves.
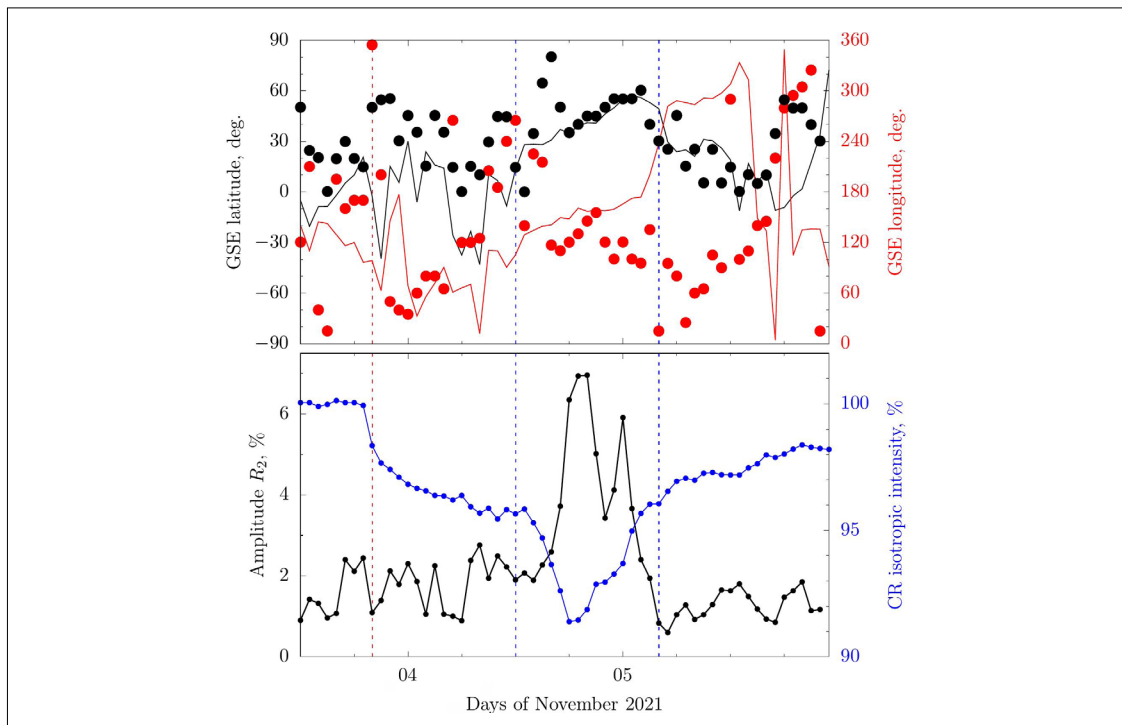

Fig. 4: Spatial angular distribution of CRs and the direction of the IMF in the space during the FD of November 3–5, 2021. The upper panel is the longitude and latitude in the in the geocentric solar ecliptic coordinate system of the direction of the IMF intensity vector (solid curves) and the second harmonic of the CR angular distribution (dots). The lower panel shows the isotropic intensity and amplitude of the second harmonic of the CR distribution. The moments of arrival of the interplanetary CME to the Earth and the boundaries of the magnetic cloud are indicated by vertical red and blue dotted lines, respectively.

profile of the second step of the FD is not typical and corresponds to the parabolic type. In other words, the phases of the decline and recovery of the CR intensity have approximately the same duration. Moreover, the direction of the maximum of tensor anisotropy and IMF in the MC region also show similar values. It can be concluded that, in the event under consideration, MC has a strong modulating effect on CR, leading to both a deep FD and a pronounced anisotropic CR distribution. It is also fair to assume that the motion of particles in the MC occurs predominantly along the force lines of the MC field.

According to the theoretical concepts of the formation of a phase transition in MC (Petukhova et al. 2019), the time profile of the decrease in the isotropic CR intensity that we found is expected. In this work, an electromagnetic mechanism for the formation of a phase transition in MC is proposed. In particular, the inductive electromagnetic field resulting from the motion of the MC leads to energy losses of positively charged particles quasi-trapped in it. In this case, the depth of modulation depends on the duration of the particle's stay inside this magnetic loop structure. It is interesting that, according to numerical calculations (Petukhova et al. 2020), the FD time profile does not depend on the structure of the magnetic field of the loop, and the anisotropy formed in it, on the contrary, is strictly determined by it. Also, in this work, it is shown what kind of CR anisotropy should be observed in MC. It is important to note that the theory predicts that a large bidirectional anisotropy should be observed in the MC. It can be assumed that our results confirm the above theory.

Acknowledgements

References

Yu, X.X., Lu, H., Le, G.M., Shi, F. 2010, Influence of magnetic cloud on variations of cosmic rays in November 2004, Solar Phys., 263, 223–237, https://doi.org/10.1007/s11207-010-9522-7

Belov, A., Abunin, A., Abunina, M., Eroshenko, E., Oleneva, V., Yanke, V., Papaioannou, A., Mavromichalaki, H. 2015, Galactic cosmic ray density variations in magnetic clouds, Solar Phys., 290, 1429–1444, https://doi.org/10.1007/s11207-015-0678-z

Burlaga, L., Sittler, E., Mariani, F., Schwenn, R. 1981, Magnetic loop behind an interplanetary shock: Voyager, Helios, and IMP 8 observations, J. Geophys. Res. Space Phys., 86(A8), 6673–6684, https://doi.org/10.1029/JA086iA08p06673

Altukhov, A.M., Krysmky, G.F., Kuzmin, A.I. 1970, The method of "global survey" for investigating cosmic ray modulation, Acta Physica Academiae Scientarium Hungaricae, 29(4), 457–460, https://articles.adsabs.harvard.edu/pdf/1970ICRC...11d.457A (last accessed June 27, 2023)

Belov, A.V., Eroshenko, E.A., Yanke, V.G., Oleneva, V.A., Abunina, M.A., Abunin, A.A. 2018, Global survey method for the world network of neutron monitors, Geomagn. Aeron., 58, 356–372, https://doi.org/10.1134/S0016793218030039

Dvornikov, V.M., Sdobnov, V.E. 1998, Analyzing the solar proton event of 22 October 1989, using the method of spectrographic global survey, Solar Phys., 17, 405–422, https://doi.org/10.1023/a:1005069806374

Bieber, J.W., Evenson, P. 1998, CME geometry in relation to cosmic ray anisotropy, Geophys. Res. Lett., 25, 2955–2958, https://doi.org/10.1029/98GL51232

Krymsky, G.F., Altukhov, A.M., Kuz'min, A.I., Krivoshapkin, P.A., Skripin, G.V., Chirkov, N.P. 1966, Cosmic ray distribution

and receiving vectors of detectors. Geomagnetizm i Aeronomiya [Geomagnetism and Aeronomy], 6, 991–996 (in Russian)

Grigoryev, V.G., Starodubtsev, S.A., Isakov, D.D. 2014, The energy spectrum of Forbush decreases during the growth phase of solar cycle 24, Geomagn. Aeron., 54, 282–286, https://doi.org/10.1134/S0016793214030062

Kravtsova, M.V., Sdobnov V.E. 2013, Rigidity spectrum of cosmic ray variations over the periods of large forbush decreases during solar cycles 22 and 23, Journal of Physics: Conference Series, 409, 012145, https://doi.org/10.1088/1742-6596/409/1/012145

Alania, M.V., Wawrzynczak, A., Sdonov, V.E., Kravtsova, M.V. 2013, Temporal changes in the rigidity spectrum of Forbush decreases based on neutron monitor data, Solar Phys., 286 ,561–576, https://doi.org/10.1007/s11207-013-0273-0

Sakakibara, S., Munakata, K., Nagashima, K. 1985, Rigidity spectrum of Forbush decrease, Proceedings from the 19th International Cosmic Ray Conference, 5, 238–241, https://articles.adsabs.harvard.edu/pdf/1985ICRC...19e.238S (last accessed June 27, 2023)

Ahluwalia, H.S., Riker, J.F. 1987, Secular changes in the upper cut-off rigidity of the solar diurnal anisotropy of cosmic rays, Planet. Sp. Sci., 35, 39–43, https://doi.org/10.1016/0032-0633(87)90142-5

Jacklyn, R.M., Duggal, S.P., Pomerantz, M.A. 1970, The spectrum of the cosmic ray solar diurnal modulation, Proc. 11th ICRC, 29, 47-54, https://articles.adsabs.harvard.edu/pdf/1970ICRC...11b..47J (last accessed June 27, 2023)

Pomerantz, M.A., Duggal, S.P. 1971, The cosmic ray solar diurnal anisotropy, Space Sci. Rev., 12, 75–130, https://doi.org/10.1007/BF00172130

Hall, D.L., Duldig, M.L., Humble, J.E. 1997, Cosmic-ray modulation parameters derived from the solar diurnal variation. ApJ, 482, 1038-1049, https://doi.org/10.1086/304158

Gololobov, P.Yu., Grigoryev, V.G., Krymsky, G.F., Gerasimova, S.K. 2021, Dynamics of energetic spectrum of solar-diurnal variations of cosmic rays in 19-24 solar activity cycles, Cosmic ray studies with neutron detectors, NMDB@Home 2020, Kiel University Publishing, 1, 43–48, https://doi.org/10.38072/2748-3150/p6

Krivoshapkin, P.A., Krymsky, G.F., Kuzmin, A.I., Skripin, G.V., Metlyaeva, E.A. 1970, The second spherical harmonics in the distribution of cosmic rays, Acta Physica Academiae Scientarium Hungaricae, 29, 147–151, 1970, https://adsabs.harvard.edu/full/1970ICRC....2..147K (last accessed June 27, 2023)

Zusmanovich, A.G., Mirkin, L.A. 1983, Energy spectrum of the semidiurnal variation of cosmic rays, Proceedings from the 18th International Cosmic Ray Conference, Bangalore, India, 3, 333-336, https://adsabs.harvard.edu/full/1983ICRC....3..333Z (last accessed June 27, 2023)

Ahluwalia, H.S., Fikani, M.M. 1996, Cosmic ray solar semidiurnal anisotropy: 1. Treatment of experimental data, JGR: Space Phys., 101(A5), 11075–11086, https://doi.org/10.1029/96JA00320

Petukhova, A.S., Petukhov, I.S., Petukhov, S.I. 2019, Theory of the formation of forbush decrease in a magnetic cloud: Dependence of Forbush decrease characteristics on magnetic cloud parameters, The ApJ, 880(1):17, https://doi.org/10.3847/1538-4357/ab2889/meta

Petukhova, A.S., Petukhov, I.S., Petukhova, S.I. 2020, Forbush decrease characteristics in a magnetic cloud. Geomagn. Aeron., 18(12), 1542–7390, https://doi.org/10.1029/2020SW002616

Open Access